# Sensing biological materials with differential RF broadband and resonating microsensors

Josephine Pichereau, Zied Fritiss, Hakim Takhedmit, Patrick Poulichet, Laurent Lanquetin, Olivier Français, Elodie Richalot

# Sensing biological materials with differential RF broadband and resonating microsensors

Josephine Pichereau[1], Zied Fritiss[1,2], Hakim Takhedmit[1], Patrick Poulichet[1], Laurent Lanquetin[2], Olivier Français[1], Elodie Richalot[1]
(1) Univ Gustave Eiffel, CNRS, ESYCOM, F-77454 Marne-la-Vallée, France
(2) Segula Technologies, pôle d'activité Pissaloup, 8 Av. Jean d'Alembert, 78190 Trappes France
josephine.pichereau@univ-eiffel.fr, zied.fritiss@segula.fr, hakim.takhedmit@univ-eiffel.fr, patrick.poulichet@esiee.fr, laurent.lanquetin@segula.fr, olivier.francais@esiee.fr, elodie.richalot-taisne@univ-eiffel.fr

***Abstract*—This paper presents two dielectric sensors dedicated to biological sample diagnostic. The first one is a resonating sensor for the characterization of small liquid sample. The second one is a broadband non-invasive sensor sub-mm spatial resolution for melanoma detection. In both cases, a differential approach is adopted in order to enhance the sensor sensitivity by limiting the impact of ambient factors (skin thickness, temperature, humidity…).**

***Keywords—complex permittivity extraction, biological tissues, non-invasive diagnostic***

## I. INTRODUCTION

Due to the permittivity variation of the biological samples versus their state, dedicated sensors can be of help in the diagnostic step. One encountered difficulty is however the influence of other factors related to the measurement environment of the patient state. Therefore, the use of a reference sample in the same conditions than the sample under test is of a great interest in order to increase the sensor accuracy and fiability.

The first sensor presented concerns applications for the analysis of small liquid samples and uses interaction of the matter with RF waves. To enhance the sensor sensitivity, a resonating structure (resonance around 1.35 GHz) has been selected. Its design is based on the symmetrical excitation of two Split Ring Resonators (SRR) loaded by the sample under test [1]. The use of two resonators permits to consider a reference liquid and to detect small permittivity variations in regard to this reference.

The second sensor uses permittivity variation between healthy skin and melanoma, to analyze a suspicious area [2]. A small sensing area (in the millimeter range) is necessary to detect tumors at its beginning of their development [3] and a good sensitivity is required to distinguish several types of lesions due to characteristics in permittivity dependence [4]. As the skin properties vary versus the body parts, individuals or the physiological conditions, in that applications, a broadband device (form 1 to 6 GHz) has been chosen and differential approach has been adopted to differentiate tumors from healthy skin in order to reduce influence of measurement environment.

## II. RESONATING STRUCTURE IN TRANSMISSION FOR SMALL SAMPLE ANALYSIS

### *A. Sensor design*

#### *a) Presentation*

The proposed sensors operates in transmission mode and contains a micro-strip line symmetrically loaded by two rectangular split ring resonators (rectangular-SRR) made of copper and printed on a substrate Arlon 25N with dielectric constant and loss tangent of 3.32 and 0.0025, respectively at 1.35 GHz. The copper thickness is of 35 µm and the substrate height given by the manufacturer of 1.6 mm. From these data, the width of the micro-strip line has been chosen to ensure impedance matching to 50 Ω. The prototypes of the two considered sensor versions, for respectively liquid and solid samples, are shown in Fig.1. The dimensions of the sensor are presented in Table I.

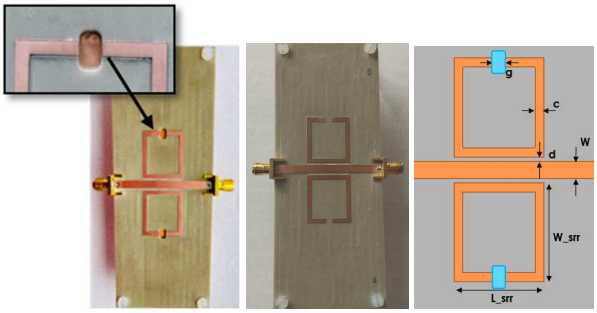


Fig. 1. Fabricated and measured sensors: microstrip structure with two ring resonators for small liquid sample (left) and for solid sample (middle). Geometrical parameters of the sensor are given in the right drawing.

TABLE I. DIMENSIONS OF THE SENSOR

| | L_srr | W_srr | d | c | g | W |
|---|---|---|---|---|---|---|
| **Size in mm** | 20 | 22 | 1 | 2 | 3 | 3.6 |

The rectangular Split Ring Resonator (SRR) can be modeled as the association of an inductance and a capacitor, the later principally depending on the gap (g = 3 mm) within the resonator. When the material under test is placed in the gap of the SRR, the gap equivalent capacitance is modified that subsequently leads to a modification of the resonant frequency [5]. Two sensor design have been developed in order to measure liquid or solid samples. For the structure on a left in Fig 1, at the gaps of both resonators, the substrate was dug and the liquids under test have been placed within these cavities to benefit from the strongest electric field amplitudes within the substrate [2]. Thus, the liquid samples under test are introduced directly inside the fabricated holes for a volume of 23 µL per hole. For the sensor on the middle of Fig 1, the sizes are the same as the previous one however the substrate was not dug to simplify the measurement for a solid sample. Using two SRRs permits to realize two different

types of measurements instead of just one when using only one SRR. Two SRRs are used in order to obtain a strong coupling and to measure the lowest possible $S_{21}$ at the resonance [6]. When the two SRRs are loaded symmetrically (with the same sample in each gap) the filtering obtained is better than with one single SRR. When the two SRRs are loaded asymmetrically, one SRR can be used as a reference which reduces the impact of the environment on the measurement results [7, 8].

*b) Analysis of gap dimensions*

To improve the performance of the sensor, various parametric studies were carried out, in particular at the level of the detection zone of the sensor. Simulations are performed using Ansys HFSS software. The sensor is simulated with its 3.5 mm SMA connectors, and radiation conditions have been applied at the boundaries. The S-parameters have been simulated over the frequency band from 1 GHz to 1.5 GHz.

Fig. 2. shows the simulation results of a parametric study of the gap, named as g, in the case of an empty sensor or when both holes are symmetrically totally filled with deionized water. Table II indicates in each case, the volume of sample, the minimal value of the transmission coefficient and the resonance frequency without sample as a function of g. According to this figure, the minimal transmission is easy to detect in all cases. In Table III, the frequency difference Sfr between both loading conditions is higher with the biggest volume which is the highest value of g. A trade-off has been made to analyze small liquid samples and to respect constraints of fabrication and measurement. In this end, the dimension g = 3 mm has been chosen.

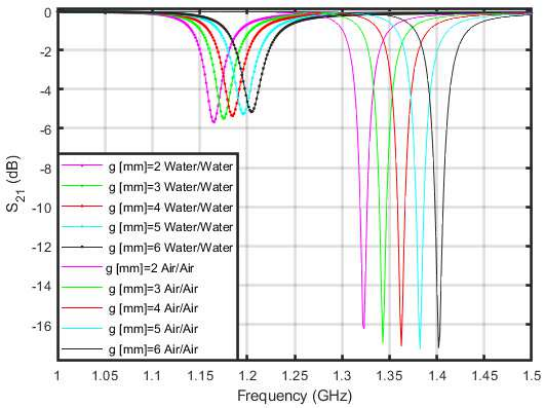


Fig. 2. Parametric study of the variation of the transmission parameter versus g value, in the case of an empty sensor or when loaded by deionized water (simulation results).

TABLE II. STUDY OF PARAMETERS AS A FUNCTION OF THE GAP

| g (mm) | 2 | 3 | 4 | 5 | 6 |
|---|---|---|---|---|---|
| Volume ($mm^3$) | 12 | 23 | 37 | 55 | 75 |
| $Sfr$ (MHz) | 158 | 160 | 188 | 186 | 196 |
| S21 Air (dB) | -16.2 | -17 | -17.1 | -17.3 | 17.2 |
| S21 Water (dB) | -5.67 | -5.45 | -5.3 | -5.27 | -5.15 |

*B. Simulation*

To study the response of the sensor for different materials, a total of 5 materials have been chosen: air, acetone, ethanol, methanol and deionized water. Their complex relative permittivity is calculated using the Debye formula:

$$\varepsilon^*_r = \varepsilon_\infty + \frac{\varepsilon_S - \varepsilon_\infty}{1 + j\frac{f}{f_0}} \quad (1)$$

Where $\varepsilon_\infty$ , $\varepsilon_s$ and $f_0$ respectively correspond to the permittivity at high frequency, the permittivity at low frequency and the relaxation frequency with respect to frequencies *f*. These parameters at 25°C for those liquids are available in [9] and listed in Table III, along with the real part of the relative permittivity of these liquids at 1.35 GHz (resonant frequency of the unloaded sensor).

TABLE III. PARAMETERS OF DEBYE FOR DIFFERENT LIQUIDS AT 25°C AND REAL PART OF THE RELATIVE PERMITTIVITY AT 1.35 GHZ

| | $\varepsilon_\infty$ | $\varepsilon_s$ | $f_0$ (GHz) | $\varepsilon_r$ at 1.35GHz |
|---|---|---|---|---|
| **Deionized Water** | 78.36 | 5.20 | 19.24 | 78.03 |
| **Methanol** | 32.66 | 5.56 | 3.14 | 28.74 |
| **Acetone** | 20.59 | 4.21 | 27.44 | 20.55 |
| **Ethanol** | 24.43 | 4.5 | 0.964 | 11.52 |

*a) Symmetrical configuration: two holes filled in*

Fig. 3 shows the simulated transmission coefficients obtained in case of unloaded sensor ("Air") and for the four liquid samples. The resonant frequency obtained varies as a function of the dielectric properties (complex permittivity) of the material under test. The frequency shift in regard to the unloaded case is called Sfr in the following. As expected, the higher is the permittivity of a material, the lower is the resonant frequency and thus the higher the frequency shift Sfr between the loaded and unloaded cases.

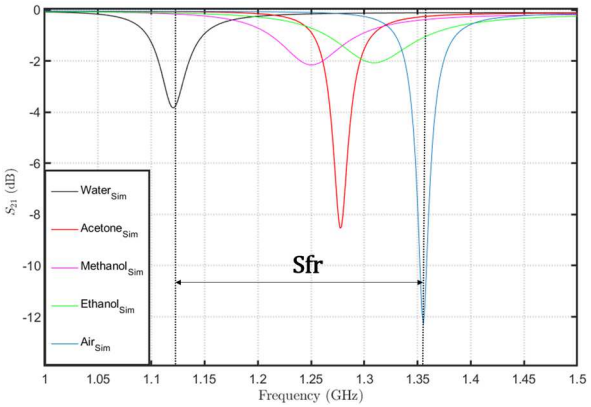


Fig. 3. *Simulated transmission coefficient $S_{21}$ versus frequency when both holes are filled in for each liquid sample.*

*b) Asymmetrical configuration: one single loaded hole*

Fig. 4 represents the simulated transmission coefficients obtained with one hole empty and one hole filled in with the four different liquid samples. Due to the dissymmetry of the sensor, two resonances appear; the highest one, related to the unloaded resonator, remains stable when the liquid changes

whereas the position of the lowest one depends on the liquid under test and decreases as the permittivity increases. Thus, this configuration offers a second fixed resonance peak that serves as a reference. This structure is designed to operate as a differential sensor and the chosen metric or indicator is the frequency difference between both resonance frequencies Δfr.

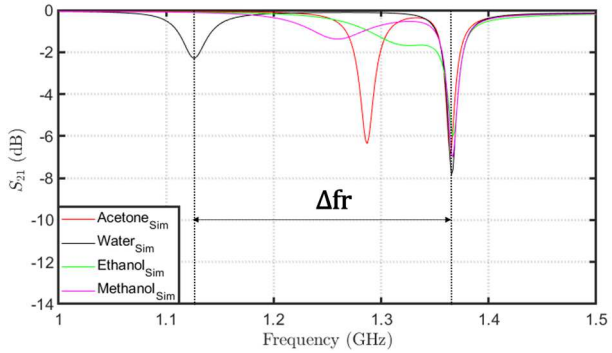


Fig. 4. *Simulated transmission coefficient $S_{21}$ versus frequency when one hole is filled in and the other one is empty, for each liquid sample.*

## C. Measurement

In order to validate the simulated prototype, it has been fabricated using LPKF Protomat S100 micro-etching machine with a substrate Arlon 25N. The measurements of the transmission coefficient $S_{21}$ have been made using a Vector Network Analyzer ZNB8 from Rohde & Schwarz. Both configurations have been considered with one or two sides loaded by the liquids under test.

In Fig 5, the measured and simulated transmission coefficient have been compared for unloaded sensors ("Air"). As shown in Table IV, the minimum transmission and the resonance frequency for both measurement and simulation are very close.

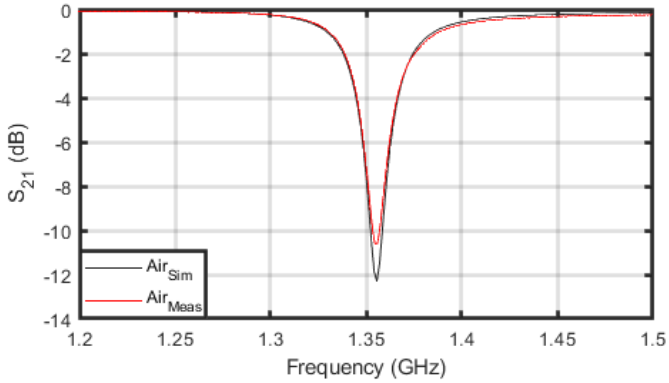


Fig. 5. *Measured and simulated transmission coefficient $S_{21}$ versus frequency when unloaded sensor*

TABLE IV. COMPARAISON BETWEEN MEASUREMENT AND SIMULATION FOR FREQUENCY SHIFT AND TRANSMISSION COEFFICIENT MINIMUM IN THE SYMETRICAL CONFIGURATION

| | **Sfr (MHz)** | |
|---|---|---|
| | Sim | Meas |
| **fr (GHz)** | 1.36 | 1.36 |
| **S21 (dB)** | -12.1 | -10.37 |

*a) Measurement results in the symmetrical configuration and comparison with simulation.*

Fig. 6 shows the measured transmission coefficient obtained in the symmetrical configuration. A shift of the resonant frequency versus the liquid under test is clearly observed. Even if there are some differences between simulated and measured curves, the shape of the curves remains similar. The resonant peaks appear along the frequency axis according to the same order in simulation and measurement with, from right to left, air, ethanol, acetone, methanol and deionized-water corresponding to the order of the real parts of their permittivity from the lowest one to the highest one.

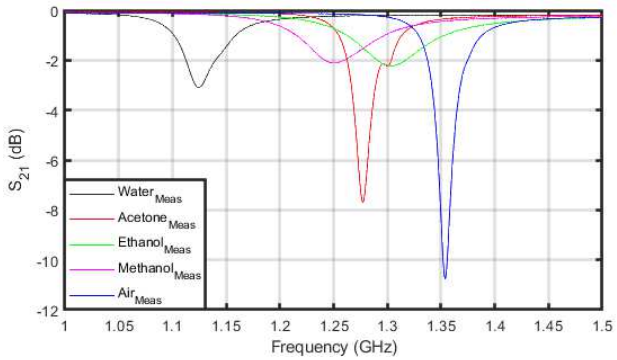


Fig. 6. *Measured transmission coefficient $S_{21}$ versus frequency when both holes are filled in for each liquid sample.*

For a more precise comparison of simulation and measurement results, Table V indicates the frequency shift Sfr in regard to the empty sensor along with the minimal value of the transmission coefficient in the case of the symmetrically filled sensor. According to Table V, measurement and simulation results are coherent in all cases. The simulated and measured frequency shifts are in the same ascending order. The difference can be explained by slight manufacturing defects of the sensor but also by difficulties to introduce the same volume of sample in each hole in measurement. In particular, some materials as acetone present a high evaporation rate that complicates the measurement procedure.

TABLE V. COMPARAISON BETWEEN MEASUREMENT AND SIMULATION FOR FREQUENCY SHIFT AND TRANSMISSION COEFFICIENT MINIMUM IN THE SYMMETRICAL CONFIGURATION

| | **Sfr (MHz)** | | **S21 (dB)** | |
|---|---|---|---|---|
| | Sim | Meas | Sim | Meas |
| **Water** | 235 | 230 | -3.83 | -3.09 |
| **Methanol** | 105 | 102 | -2.15 | -2.12 |
| **Acetone** | 78.4 | 76.6 | -8.54 | -7.69 |
| **Ethanol** | 49 | 49 | -2.06 | -2.22 |

*b) Measurement results in the asymmetrical configuration and comparison with simulation.*

Fig. 7 shows the measured transmission coefficient obtained in the asymmetrical configuration. It can be seen that, as in simulation, there is a fixed peak that can serve as a reference and a peak moving as the liquid under test changes.

Table VI presents the difference Δfr between both resonance frequencies along with the minimal transmission coefficient value at the lowest resonance frequency when one hole is empty. The frequency differences between both

resonances obtained through simulation and measurement are in the same ascending order. Frequency differences obtained through measurement are however lower than those obtained by simulation. As with the previous configuration, the repeatability of measurements is difficult to get due to the effective filling of the holes with the same volume of sample as in simulation. The comparison of the results obtained in both configurations shows that the symmetrical case achieves a deeper transmission minimum than the asymmetrical case, as might be expected. Furthermore, in the asymmetrical case, the frequency differences are of the same order of magnitude in measurement and simulation.

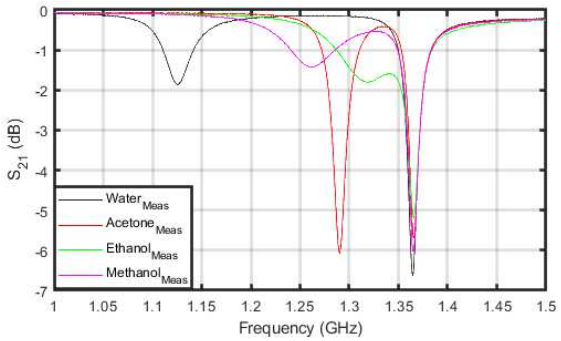


Fig. 7. *Measured transmission coefficient $S_{21}$ versus frequency when one hole is filled in and the other one is empty, for each liquid sample.*

TABLE VI. COMPARAISON BETWEEN MEASUREMENT AND SIMULATION FOR FREQUENCY DIFFERENCE BETWEEN BOTH RESONANCES AND LEFT PEAK TRANSMISSION COEFFICIENT MINIMUM IN THE ASYMETRICAL CONFIGURATION

| | **Δfr (MHz)** | | **S21 (dB)** | |
|---|---|---|---|---|
| | Sim | Meas | Sim | Meas |
| **Water** | 239 | 239 | -2.288 | -1.86 |
| **Methanol** | 111 | 99.2 | -1.377 | -1.43 |
| **Acetone** | 77 | 76.1 | -6.362 | -6.06 |
| **Ethanol** | 53 | 48.5 | -1.62 | -1.8 |

## III. BROADBAND PCB-BASED COAXIAL SENSOR FOR SKIN SCREENING

The second sensor is a broadband skin sensor operating between 1 and 6 GHz and it has been designed in order to detect cutaneous permittivity variations indicating the development of a tumor. It consists of an open-ended probe whose sensing area mimics a coaxial probe [10] and is connected to a SMA connector through a stripline in Fig. 7. The sensitive part is printed on a 1.52 mm thick Rogers 3003 substrate ($\varepsilon r$ = 3.00 and $\tan\delta$ = 0.0010 at 10 GHz) whereas two 1.524 mm thick Arlon 25N substrates ($\varepsilon r$ = 3.32 and $\tan\delta$ = 0.0025 at 10 GHz) are used to form the stripline access. To obtain a coaxial-like sensitive area, the metallization is removed on a 2.3 mm diameter circular area in purple in Fig. 8, a 0.5 mm diameter metallized vias is inserted as a central conductor, and eight 0.5 mm metallized vias are added to mimic the outer conductor and improve the sensor resolution. The small diameter of the sensing area enables the examination of small surfaces consistent with skin heterogeneity imaging; indeed, the diameter of the circular area where the metallization is removed (of 2.3 mm) is smaller than the average size of a melanoma lesion (around 6 mm).

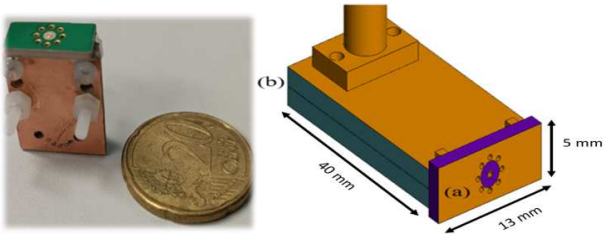


Fig. 8. *Sensor prototype (left) and 3D-view (right) with (a) the open-ended sensitive area, (b) the SMA connector to stripline transition.*

A permittivity extraction method suited for open-ended sensors [11] permits to extract the permittivity of the material under test after a calibration step implying the measurement of three samples of known permittivity. The capability of this sensor to retrieve with a good accuracy the permittivity of the material under test over the whole 1 GHz-6 GHz frequency band has been shown [12]. Following the process proposed in [13], skin phantom tissues of different properties have been fabricated and the ability of the sensor to distinguish different tissues has been tested [12].

To simplify the use of this sensor by medical practitioners, an alternative approach avoiding the calibration step has been proposed. This differential approach consists of a comparison of the complex reflection coefficients measured on a patient at two close locations respectively corresponding to safe skin (considered as a reference) and a suspicious lesion. The used indicator is calculated as $\Delta S_{11} = |S_{11MUT} - S_{11ref}|$ while comparing the reflection coefficient obtained for the material under test (MUT) and for the reference material (ref). Measurements performed on different phantom tissues show the sensitivity of the proposed indicator in Fig. 9.

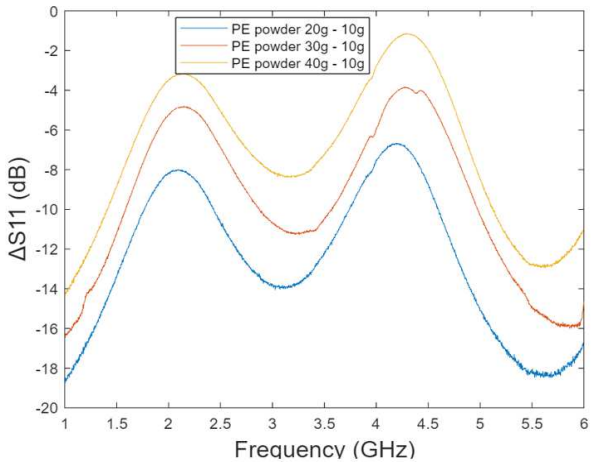


Fig. 9. *Measurement results of the difference between the complex reflection coefficients with several PE powder-based phantoms, for a reference material obtained using 10g of PE powder.*

## IV. MEASUREMENT ON TUMOR PHANTOM TISSUES USING BOTH SENSORS

Using the process presented in [12], samples reproducing the dielectric properties of melanoma has been fabricated. Measurements have been simultaneously performed using the coaxial sensor and the resonating sensor for solid samples. The real and imaginary parts of the relative permittivity extracted from the measurements using the coaxial sensor are presented in Fig. 10.

These extracted values at 1.35 GHz have been used to simulate the resonator sensor loaded by the same material.

Fig. 11 shows a comparison of the simulated and measured transmission parameters when the resonating sensor is symmetrically or asymmetrically loaded by this phantom tissue. The similar frequency shift obtained in simulation and measurement indicates coherent responses of both sensors.

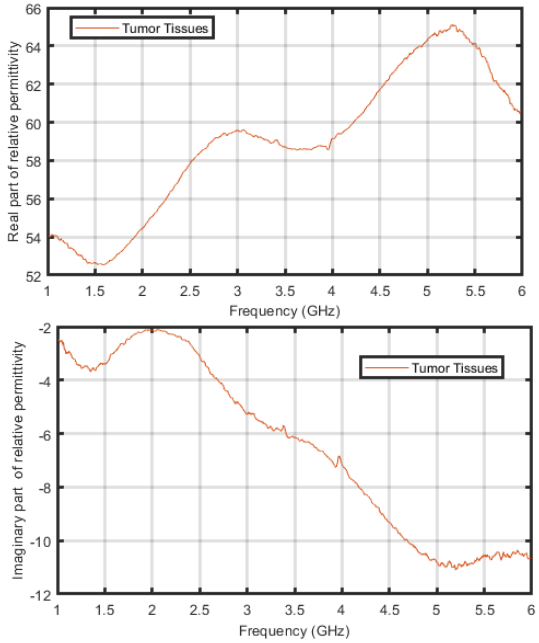


Fig. 10. *Real and imaginary parts of the tumor tissue permittivity extracted using the open-ended sensor.*

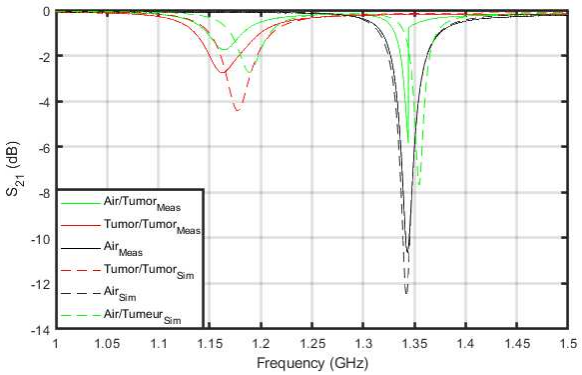


Fig. 11. *Simulated and measured transmission coefficient $S_{21}$ versus frequency with tumor sample on the resonating sensor.*

TABLE VII. SIMULATED AND MEASURED RESULTS WITH THE PHANTOM TISSUE ON THE RESONATING SENSOR IN BOTH CONFIGURATIONS

| | **Tumor** | |
|---|---|---|
| **Symmetrical configuration** | Sim | Meas |
| **Δfr (MHz)** | 165 | 181 |
| **S21 (dB)** | -4.41 | -2.7469 |
| | | |
| **Asymmetrical configuration** | Sim | Meas |
| **Sfr (MHz)** | 164 | 180.5 |
| **S21 (dB)** | -2.72 | -1.7521 |

## V. CONCLUSION

This paper presents two sensors dedicated to biological diagnostic applications.

The first one concerns a resonant design operating in transmission mode around 1.35 GHz and dedicated to characterize the dielectric properties of small volumes of liquids and solid biological samples. Both in simulation and in measurement, a shift of the resonance frequencies linked to the permittivity of the samples under test is observed with a good concordance. Whereas an asymmetry in the sensor loading leads to the appearing of two resonance peaks, it could permit to determine small composition variations between a reference liquid and a liquid under test; this property could be of interest for disease diagnostic.

The second one has been designed in order to probe, in the [1 GHz ; 6GHz] frequency band, small skin surfaces in regard to melanoma lesion size and permits to distinguish safe skin from tumor with a good accuracy. The fabrication of tumor phantom samples has permitted to verify the coherence of the results obtained using both sensors.

## ACKNOWLEDGMENT

The authors thank Stéphane Protat from ESYCOM/UGE for the fabrication of coaxial sensors and his involvement in these two different projects and Jimmy Leszczynski from ESYCOM/UGE for the fabrication of microstrip sensors.

## REFERENCES

[1] A. A. M. Bahar, Z. Zakaria, A. A. M. Isa, Y. Dasril and R. A. Alahnomi, "Dielectric properties measurement based on split ring resonator for microfluidic characterization," *12th European Conference on Antennas and Propagation (EuCAP 2018)*, London, UK, 2018, pp. 1-5, doi: 10.1049/cp.2018.1051

[2] Mirbeik-Sabzevari, Amir, Robin Ashinoff, and Negar Tavassolian. "Ultra-wideband millimeter-wave dielectric characteristics of freshly excised normal and malignant human skin tissues." IEEE Transactions on Biomedical Engineering 65.6 (2017): 1320-1329.

[3] Mohammed B J, Naqvi S A R, Manoufali M, Bialkowski Kand Abbosh A M 2018 Changes in epidermal dielectric properties due to skin cancer across the band 1–50 GHz 2018 Australian Microwave Symp. (AMS) (IEEE)

[4] Naqvi S A R, Mobashsher A T, Mohammed B, Foong D and Abbosh A 2023 Benign and malignant skin lesions: dielectric characterization, modelling and analysis in frequency band 1–14 GHz IEEE Trans. Biomed. Eng. 70 628–39

[5] W. Withayachumnankul, K. Jaruwongrungsee, A. Tuantranont, C. Fumeauxa, D. Abbott, "Metamaterial-based microfluidic sensor for dielectric characterization", Sensors and Actuators A 189 (2013) 233–237

[6] G. Galindo-Romera, F. Javier Herraiz-Martínez, M. Gil, J. J. Martínez-Martínez and D. Segovia-Vargas, "Submersible Printed Split-Ring Resonator-Based Sensor for Thin-Film Detection and Permittivity Characterization," in *IEEE Sensors Journal*, vol. 16, no. 10, pp. 3587-3596, May15, 2016, doi: 10.1109/JSEN.2016.2538086K. Elissa, "Title of paper if known," unpublished.

[7] S. Mohammadi, A. V. Nadaraja, K. Luckasavitch, M. C. Jain, D. J. Roberts and M. H. Zarifi, "A Label-Free, Non-Intrusive, and Rapid Monitoring of Bacterial Growth on Solid Medium Using Microwave Biosensor," in *IEEE Transactions on Biomedical Circuits and Systems*, vol. 14, no. 1, pp. 2-11, Feb. 2020, doi: 10.1109/TBCAS.2019.2952841

[8] A. Ebrahimi , J. Scott , and K. Ghorbani, "Differential Sensors Using Microstrip Lines Loaded With Two Split-Ring Resonators", IEEE SENSORS JOURNAL, VOL. 18, NO. 14, JULY 15, 2018

[9] H. Mariam, P. Poulichet, H. Takhedmit, E. Richalot and O. Francais, "Dielectric Spectroscopy Characterization within a Microfluidic Device based on Open-Ended Coplanar Waveguide," *2020 14th European Conference on Antennas and Propagation (EuCAP)*,

Copenhagen, Denmark, 2020, pp. 1-5, doi: 10.23919/EuCAP48036.2020.9135471

[10] A. La Gioia, E. Porter, I. Merunka, A. Shahzad, A. Salahuddin, M. Jones, & M. O'Halloran "Open-ended coaxial probe technique for dielectric measurement of biological tissues: Challenges and common practices." Diagnostics 8.2 (2018): 40.

[11] N. Wagner, M. Schwing and A. Scheuerman, "Numerical 3D FEM and experimental analysis of the open-ended coaxial line technique for microwave dielectric spectroscopy on soil", in IEEE Trans. Geosci. Remote Sens., 2013, vol. 52, no 2, p. 880-893.

[12] M. Z. Fritiss, P. Poulichet, H. Takhedmit, L. Lanquetin, S. Protat, P. Vallade, E. Richalot, O. Français, "Design and characterization of a broadband PCB-based coaxial sensor for permittivity screening in skin cancer detection applications", Meas. Sci. Technol. **34** 115109 (DOI 10.1088/1361-6501/ace9f1).

[13] R. Aminzadeh, M. Saviz and A. A. Shishegar, "Characterization of low-cost tissue mimicking materials at millimeter-wave frequencies," 23rd Iranian Conference on Electrical Engineering, 2015, pp. 283-287, doi: 10.1109/IranianCEE.2015.7146225.